Directed network of substorms using SuperMAG ground-based magnetometer data

L.Orr[1], S.C.Chapman[1], and J.W.Gjerloev[2,3]

[1]Centre for Fusion, Space and Astrophysics, University of Warwick, UK
[2]Applied Physics Laboratory- John Hopkins University, Laurel, Maryland, USA
[3]Birkeland Centre, University of Bergen, Norway

Key Points:

- First dynamical network analysis of substorm current systems that is directed, quantifying both formation and expansion.
- Full spatio-temporal pattern from 86 isolated substorms obtained using the 100+ SuperMAG ground based magnetometers and Polar VIS.
- Identified timings of a consistent sequence in which the classic substorm current wedge forms.

This article has been accepted for publication and undergone full peer review but has not been through the copyediting, typesetting, pagination and proofreading process which may lead to differences between this version and the Version of Record. Please cite this article as doi: 10.1029/2019GL082824

Corresponding author: L.Orr, L.Orr@warwick.ac.uk

Abstract

We quantify the spatio-temporal evolution of the substorm ionospheric current system utilizing the SuperMAG 100+ magnetometers. We construct dynamical directed networks from this data for the first time. If the canonical cross-correlation (CCC) between vector magnetic field perturbations observed at two magnetometer stations exceeds a threshold, they form a network connection. The time lag at which CCC is maximal determines the direction of propagation or expansion of the structure captured by the network connection. If spatial correlation reflects ionospheric current patterns, network properties can test different models for the evolving substorm current system. We select 86 isolated substorms based on nightside ground station coverage. We find, and obtain the timings for, a consistent picture in which the classic substorm current wedge (SCW) forms. A current system is seen pre-midnight following the SCW westward expansion. Later, there is a weaker signal of eastward expansion. Finally, there is evidence of substorm-enhanced convection.

1 Plain Language Summary

Space weather makes beautiful auroral displays (the northern and southern lights), but with these come large-scale electrical currents in the ionosphere which generate disturbances of magnetic fields on the ground. These are observed by > 100 magnetometer stations on the ground, and the challenge is to extract the important information from these many observations and present it as a few key parameters that indicate how severe the ground impact will be. Networks are now a common analysis tool in societal data, where people are linked based on various social relationships. Other examples of networks include the world wide web, where websites are connected via hyperlinks, or maps where places are linked via roads. We have constructed networks from the magnetometer observations of space weather events (geomagnetic sub-storms), where magnetometers are linked if there is significant correlation between the observations. There has been considerable debate as to how the ionospheric pattern evolves during a geomagnetic substorm. We are able to use the networks to resolve some of these controversies.

2 Introduction

Substorms, their associated current systems, and the corresponding geomagnetic displacements seen at earth, have been the subject of longstanding interest (Pulkkinen, 2015). The fundamental morphology, stages of development, and their timings are well established (Akasofu, 1964). The classic scenario is that of the formation of a substorm current wedge (SCW) (McPherron, Russell, & Aubry, 1973), a rapidly appearing, intense westward electrojet that follows disruption to the cross-tail current system. This corresponds to the DP1 pattern of magnetic perturbations in the nightside auroral zone, which appears in addition to the DP2 geomagnetic counterpart associated with the convective system in the dawn and dusk auroral zones (Nishida, 1968). However, there have been several important variants of this picture. Kamide and Kokubun (1996) proposed a two component auroral electrojet, and Sergeev et al. (2011) argued that their computational wedge model is more consistent with observations, if an additional region two polarity field-aligned current is added to the classic SCW cartoon. Gjerloev and Hoffman (2014) proposed a two-wedge current system, comprised of a bulge and an oval current wedge, in their empirical model of the ionospheric equivalent current system, during an auroral substorm. Recently it was proposed, by Liu et al. (2018), that there is no large-scale westward electrojet but rather many small, individual segments. These proposed models point to the outstanding question: what is the average substorm current system morphology that we can quantify and resolve uniquely from the full set of available ground-based magnetometer observations? The goal of this paper is to construct a method that quantifies the time-evolving spatial pattern seen across all 100+ magnetometers, in a man-

ner that allows systematic averaging across may substorm events. This will provide a quantitative benchmark to test against model predictions. Key aspects of many of the above models, whilst being physically distinctive, are qualitative. Our results place these qualitative predictions in direct contact with the observations, and can thus drive forward the formation of quantitative hypotheses that will allow these models to be distinguished.

The SuperMAG initiative (Gjerloev, 2012) makes the full set of 100+ ground-based magnetometer observations routinely available, with a standardized coordinate system and a common baseline, supporting both single event and comparative statistical studies. In this form the data is now amenable to analysis methodologies designed to quantify spatio-temporal pattern in sets of multiple, spatially distributed observations. Complex network methodology has recently grown in popularity as a useful mathematical tool and has been used to analyse complex systems from a variety of disciplines ranging from social sciences (Albert & Barabási, 2002; Newman, 2003; Watts & Strogatz, 1998) to geophysical data (Boccaletti, Latora, Moreno, Chavez, & Hwang, 2006; Malik, Bookhagen, Marwan, & Kurths, 2012; McGranaghan, Mannucci, Verkhoglyadova, & Malik, 2017; Stolbova, Tupikina, Bookhagen, Marwan, & Kurths, 2014; Wiedermann, Radebach, Donges, Kurths, & Donner, 2016). Crucially, unlike other data assimilative methods, including AMIE (Richmond & Kamide, 1988), network analysis does not introduce spatial correlation. Furthermore, our network analysis does not require any a priori assumptions for variation in ground conductivity since we normalize for this using solely the data to determine the time and station dependent network threshold.

Dods, Chapman, and Gjerloev (2015) recently demonstrated, on a small set of events, that a network methodology could be applied to the full set of magnetometers for single isolated substorms to yield a characteristic network signature of substorm onset. The networks are time-dependent, hence contain information on the timings of substorm evolution (Dods, Chapman, & Gjerloev, 2017). Canonical correlation is used to study correlations between multivariate datasets (Reinsel, 2003). If we have two vector time series, canonical correlation analysis will determine the linear combination of the two which are maximally cross-correlated. The cross-correlation between these linear combinations is the (1st) canonical cross-correlation (CCC) component. The key elements of this network analysis are (i) to calculate the CCC of the vector magnetic field time series between each pair of magnetometers and (ii) to apply a station and event specific threshold to this CCC, which is obtained directly from the data. The station pairs that have CCC above the threshold then form a time varying network.

The analysis of Dods et al. (2015), only examined the *undirected* network (zero-lag CCC). This was sufficient to reveal the initial formation of the SCW at substorm onset but without directional information could not capture the full spatio-temporal evolution of the current system. In this paper we construct the networks based on the (often non-zero) time lags at which the CCC between each pair of stations is maximal, to form the substorm *directed* network, which captures the direction of information propagation between network nodes (magnetometers). Looking across a range of CCC lags captures the full pattern of spatial correlation and how it evolves in time. Non-zero CCC lags indicate the time-scale for propagation or expansion of a coherent structure and the sign of the lag gives the direction of propagation or expansion. We construct specific sub-networks to test the hypotheses of different proposed models for how the ionospheric current system evolves. The sub-networks isolate different spatial regions and allow us to test for connections between them. We will focus on spatially well-sampled isolated substorm events and establish network parameters that characterize how the magnetometers collectively respond to the SCW. We have identified 86 events that meet the sampling requirements (this is a subset of the substorm list used in the series of papers by Gjerloev and Hoffman (Gjerloev & Hoffman, 2014; Gjerloev, Hoffman, Sigwarth, & Frank, 2007)). We find timings for a pattern in the magnetic field perturbations consistent with

the SCW formation at onset which then expands westward to form a coherent current system in the pre-midnight sector. There is additional weaker, eastward expansion of the SCW, followed by coherent correlation patterns spanning the entire nightside.

The organization of the paper is as follows. In section 3 we describe the methods and the data used to obtain the directed networks. In section 4 we highlight a case study of one substorm and present a statistical survey 86 events which reveals how on average the spatial pattern of correlation evolves as the substorm progresses. We conclude in section 5.

3 Methods

3.1 Constructing the dynamical directed network

For each substorm we first construct the full dynamical directed network before dividing it into sub-networks that flag spatial correlation within and between specific spatial regions. These regions are selected to test different proposed models of substorm current patterns. The term 'dynamical' is used here as in the networks literature (Jost, 2007). Our analysis cannot resolve short-range fine structures that are smaller than, or of the order of the inter-magnetometer spacings, but can test whether long-range spatially correlated patterns exist. The method for forming a network, at zero lag, is detailed in Dods et al. (2015). The magnetometer stations form the nodes of the network and a given pair of nodes are *connected* if the CCC of their vector magnetic field perturbation time series exceeds an event and station specific threshold, as specified in Dods et al. (2015). In summary, the CCC is calculated over a 128 minute running window of the magnetic field perturbations observed by magnetometer pairs. The data is at minute resolution, giving a 128 point CCC for each station pair, every minute. The 128 minute sliding window is chosen to give sufficient accuracy in the computed cross-correlation function whilst also capturing the large-scale spatial and temporal behaviour of the substorm current wedge. Dods et al. (2017) previously demonstrated using model time series that this window length resolves changes on timescales much shorter than that of the window, specifically capturing onset where there is a sharp ramp in activity in time as the SCW forms. A network is calculated for every minute and all times, t, will refer to the leading edge of the window, that is the last time point spanned by the window (i.e. a window spanning time interval $[T, T + 127]$ will have network properties plotted at time $t = T + 127$). Each windowed, three-component vector magnetic field time series is (1) linearly detrended and (2) the CCC is calculated for each station pair then (3) if the correlation between magnetometers i and j exceeds the maximum of the two station thresholds then they are connected and are part of the network. For a network with M active magnetometers, an $M \times M$ adjacency matrix, $\mathbf{A}$, is formed which has $\mathbf{A}_{ij} = 1$, if i and j are connected, and $\mathbf{A}_{ij} = 0$, otherwise. The station specific threshold for each magnetometer station is determined such that the station will be connected to the network for 5% of the month (28 days) surrounding the event. This ensures that all stations have the same likelihood of being connected to the network, independent of their individual sensitivities to an overhead current perturbation, which in turn depends on the individual instrument characteristics and the local time and season dependent ground conductivity.

Dods et al. (2015) constructed the network using just the CCC at zero lag. Here, we form the directed network by considering the lag at which the CCC is maximal, τ_c, up to a lag of ± 15 minutes. The value of the CCC value at lag τ_c is used to determine if the stations are connected (exceeds the threshold) and each connection then also has a direction and timescale of propagation of the observed signal, which is spatially coherent between the two stations. This potentially corresponds to the coherent pattern of time-varying ionospheric currents. The adjacency matrix, $\mathbf{A}$, is not symmetric and the sign of τ_{cij} determines the signal propagation direction for $\mathbf{A}_{ij}$. If the CCC between mag-

netometer i and j is above the threshold (they are connected), but with $\tau_c < 0$, we can infer that the signal originates at j and propagates towards i, $j \rightarrow i$. If $\tau_c > 0$ the propagation is $i \rightarrow j$.

Gjerloev (2012) found that the probability distributions of differences between SuperMAG baselines and official quiet days rarely exceed 20nT. For consistency we also exclude magnetometers from the network whose time series of magnetic field perturbations never exceed this noise level.

3.2 Data and event selection

We analyse vector magnetometer time series at 1 minute time resolution for the full set of magnetometer stations available from the SuperMAG database. This data is processed as in Gjerloev (2012), such that the ground magnetic field perturbations are in the same coordinate system, and have had a common baseline removed. A set of isolated substorm events, occurring between $1997 - 2000$, has been previously identified in Gjerloev et al. (2007). These events have been selected such that (i) they are isolated single events optically and magnetically; (ii) the onset location is spatially defined; (iii) bulge-type auroral events; (iv) there is a single expansion and recovery phase (or the end of the event is at the time of a new expansion); (v) the entire bulge region is in darkness to eliminate any terminator effects; and (vi) they are not during magnetic storms ($|Dst| < 30$nT) or prolonged magnetic activity. The requirement for darkness creates biases as the events with the majority of the nightside in darkness are in the months around winter solstice. Excluding daylit stations does however avoid large differences in ground conductivity between the stations which would otherwise dominate the CCC analysis. We also require that activity levels are low for a full window of 128 minutes before the substorm onset. Together these selection criteria, along with the requirement for a sufficient number of stations in the spatial region around onset (described below) give 86 suitably isolated substorms (listed in the SI.)

3.3 Normalization to a substorm epoch time

It is well established that substorms vary in duration (Kullen & Karlsson, 2004; Tanskanen, Pulkkinen, Koskinen, & Slavin, 2002). In order to perform an average across many events we need to map each event onto a single normalized time-base such that, once normalized, all substorms share a common onset time and take the same length of time to evolve from onset to the peak of activity. Following Gjerloev et al. (2007), the observed event time, t, is related to the normalized time, t', by:

$$t' = \frac{T_E \times (t - t_{onset})}{t_{peak} - t_{onset}} \tag{1}$$

where $T_E = 30$ minutes, approximately the average length of a substorm expansion phase. The onset time is then at $t' = 0$ and the time of peak expansion $t' = 30$. The critical timings for this normalization, t_{onset} and t_{peak}, can be unambiguously identified in these isolated substorm events.

3.4 Sub-networks for specific auroral spatial regions

We construct time-varying directed sub-networks that quantify correlation within and between specific spatial regions in the nightside. These spatial regions are selected for each event as shown in Figure 1. The network is constructed using stations located between $60-75^\circ$ magnetic latitude and within the nightside. Gjerloev and Hoffman individually determined the timings and positions of onset and the east and west ends of the bulge portion of the aurora using polar VIS images (Gjerloev et al., 2007). The LT of the bulge edges at the time of maximum expansion ($t' = 30$) have been used to define the boundaries of region B. The study was repeated using the east and west bound-

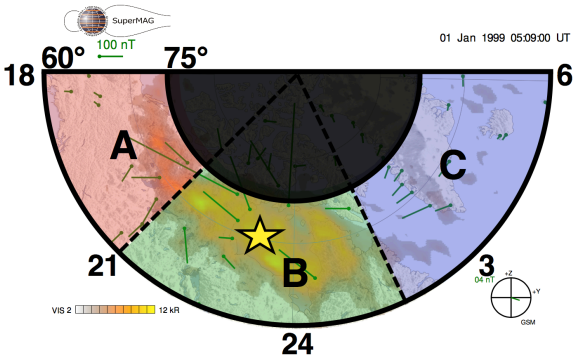

Figure 1. SuperMAG polar plot indicating the spatial regions A, B and C for which we obtain sub-networks. All data is from stations between 60 − 75° magnetic latitude, within the nightside. The LT boundaries between A, B and C are different for each event and are determined from Polar VIS images; they are separated by the east and west boundaries of the bulge at the time of maximum expansion (dashed lines). The magnetic latitude and local time of onset (again from Polar VIS) for each event, are indicated by the yellow star.

aries of the bulge fifteen normalized minutes before, and after, the maximum expansion phase ($t' = 15$ and $t' = 45$), results are presented in the SI. This gives slight differences but the overall results and conclusions are unchanged. The SCW is typically six hours of local time in extent (Gjerloev et al., 2007) which corresponds to region B; regions A and C are westwards and eastwards of the SCW respectively.

We will present a detailed study of the sub-networks for a single event and then will compare it to the average sub-network behaviour seen across all 86 isolated substorms. An event was identified which has ≥ 7 magnetometer stations in each of regions A, B and C for the duration of the substorm; this occurs on $01-\text{Jan}-1999$ with onset at $04:52$ UT. It had a relatively short expansion phase, 17 minutes, and a thin SCW, extending over 4.1 hours of LT at the time of peak expansion ($t' = 30$). For the averaged study over 86 events we require at least three magnetometers in a spatial region for it's sub-network to be included in the study. For example, a substorm in which there were ≥ 3 magnetometers in regions A and B, but < 3 in C, will contribute to the average sub-networks behaviour within A and B but not within sub-network C. We repeated the entire analysis with the more restrictive criterion of ≥ 7 magnetometers and found very similar results (see SI). One benefit of using network analysis is that we do not require a spatially uniform grid of magnetometers, that being said, the condition of having ≥ 3 magnetometers per region gives a mean spatial separation distance (within regions) of ~ 1000km.

The spatial regions A, B and C are defined such that the sub-networks are always in the same local time relative to the SCW but, as the earth rotates, the geomagnetic location of the magnetometer stations will vary. This will not affect the properties of the computed network provided regions A, B, C continue to be well-sampled with stations. However, the number of stations within each region can change. We therefore include a normalization to the number of possible connections to define the parameter that we will use to quantify the network, the normalized number of connections:

$$\alpha(t) = \frac{\sum_{i \neq j}^{N(t)} \sum_{j \neq i}^{N(t)} \mathbf{A}_{ij}}{N(t)(N(t)-1)} \tag{2}$$

where $\mathbf{A}$ is the adjacency matrix and $N(t)$ is the number of active magnetometers.

4 Results

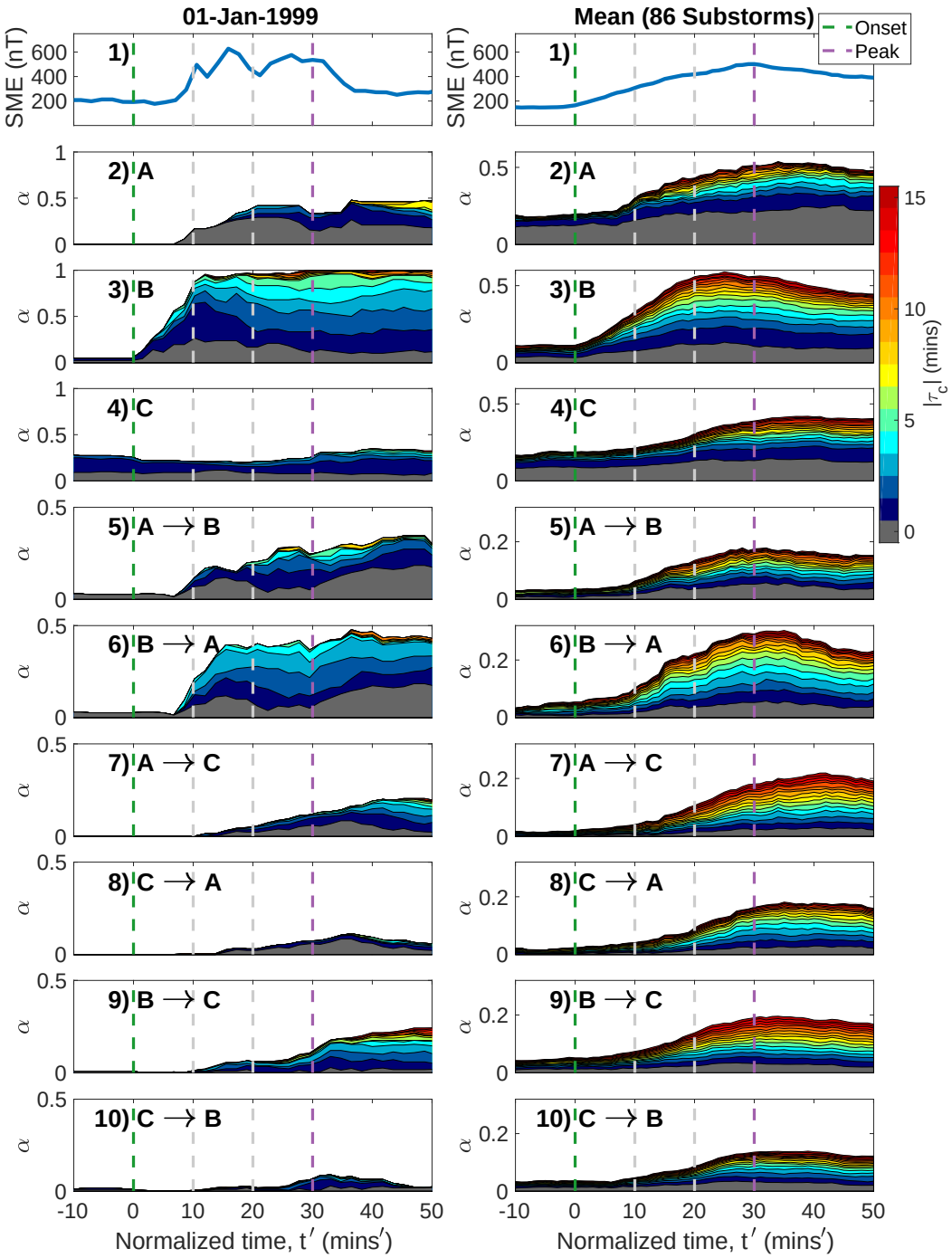

Figure 2. The normalized number of connections, $\alpha(t', \tau_c)$, is binned by the lag of maximal canonical cross-correlation (CCC), $|\tau_c|$. Each panel stacks vertically (one above the other) $\alpha(t', \tau_c)$ versus normalized time, t', for $|\tau_c| \leq 15$. $|\tau_c|$ is indicated by colour (see colour bar). Panel 1 plots the SuperMAG electrojet index, SME. Panels $2 - 10$ plot α for connections within and between each of the regions A, B and C (identified in Figure 1). The left columns plot a single event, whereas the right plots the average of 86 events (containing sub-networks with ≥ 3 magnetometers per region). Substorm onset (green dashed line) is at $t' = 0$ and the maximum of the expansion phase (purple dashed line) is at $t' = 30$.

4.1 Observed timings of spatial correlation

We now present (in figure 2) the directed network for the individual substorm identified above (left column), and the average of all 86 selected substorms (right column). Substorm evolution is not necessarily linear but the individual substorm is plotted as an example to highlight that the multi-event mean is a reasonable average. Having obtained the sub-networks for each region (identified in figure 1), we have the normalized number of connections, $\alpha(t', \tau_c)$ (equation 2) within (panels $2-4$), or between the regions A, B and C (panels $5-10$). Looking at connected magnetometers within each region provides timings of the emergence of coherent spatial patterns of correlation in the magnetic field perturbations (at ground level), whilst connections between regions provide information on how these patterns are propagating and/or expanding through out the substorm; any inter-region dependencies will also be flagged. If all possible magnetometer connections are present then $\alpha = 1$. Since the connections between regions (e.g. A→C and C→A) are plotted separately (e.g. panel 7 and 8), then if these were fully connected, the sum over the two plots would be 1. Hence the range of values for the y-axes for connections between regions (panels 5-10) are half the size of that within the regions (panels 2-4).

As the networks are constructed using the time delay/lag at which the CCC between each pair of magnetometer stations is maximal, each connection has an associated signed lag, τ_c. We bin the number of connections (α) into ranges of the magnitude of this lag (τ_c). Connections which are at zero lag have no time delay i.e. $\tau_c = 0$ (grey), and connections with an associated direction of propagation/ expansion, from one magnetometer to another, have a range of delays, that is, lags from $1-15$ minutes (blue-red). The sign of the lag indicates a direction of propagation or expansion from one magnetometer location to another; this information is combined with the physical geographical locations of the magnetometers to determine if the propagation/expansion is eastward or westward. The connections are separated into different panels for each direction and then binned by the magnitude of the lag. For example, between regions A and C, panel 7 plots the A→C propagation/expansion, eastward, from region A into region C whilst panel 8 plots C→A propagation/expansion, westward, from region C into region A. Connections with a lag $\tau_c = 0$ (indicated in grey) are plotted on both panels 7 and 8 (A→C and C→A) as they simply indicate instantaneous correlation between regions A and C, which have no associated direction and thus, by definition the grey bars are identical on the two plots.

Figure 2 stacks the time series of the normalized number of connections, $\alpha(t', \tau_c)$, so that the value of α for each range of $\mid \tau_c \mid$ are plotted one above the other for increasing $\mid \tau_c \mid$. The stacking is such that each independent $\alpha(t', \tau_c)$ is visible. The envelope is then the total (normalized) number of connections over all lags, that is, all $\mid \tau_c \mid \leq 15$. For example, during the individual substorm (left column), we see mostly instantaneous (grey) correlation within A (panel 2) with an additional low level of lagged correlation later in the substorm. On the other hand within B (panel 3), at the time of peak expansion (purple dashed line) the network is made up of $\sim 10\%$ instantaneous correlation, $\sim 80\%$ with $1 \leq \mid \tau_c \mid \leq 5$ (fast propagating or expanding) and $< 10\%$ of connections have $\mid \tau_c \mid \geq 6$ (slow expansion or propagation). The plot covers the time interval $-10 \leq t' \leq 50$ normalized minutes where the times of onset, peak expansion and the 10 minute intervals in-between are indicated with vertical dashed lines. The figure presents a summary of time-varying spatial correlation for each sub-network for the duration of the substorm. The full networks for the individual substorm are plotted in the SI. The SME (SuperMAG electrojet index) for the individual event, and its multi-event average, is plotted in panel 1 of figure 2. We can see that although the events are on a normalized time-base, the multi-event average is more smooth and responds less sharply to onset than the individual event.

Prior to onset, the multi-event average shows some spatially coherent connections within each of regions A and C (panels 2 and 4). These connections are mostly instantaneous ($\mid \tau_c \mid = 0$, grey shading) or with 1 minute lag ($\mid \tau_c \mid = 1$, dark blue shading). Importantly these regions are not correlated with each other, so that the number of A→C and C→A connections are small (panels 7 and 8). At onset, in both the individual event and the statistical average, (panel 3) we see that the sub-network within region B has the most prompt and largest response, that is, increase in spatial correlation. For the individual substorm we see a sharp increase in the number of correlated pairs, beginning at onset ($t' = 0$) and increasing to $\sim 100\%$ (all magnetometers within B are highly correlated) at $t' \sim 15$. Likewise, the multi-event average number of correlated magnetometer pairs within the B sub-network begins to increase at onset, but it is smoother and reaches a peak slightly later than in the individual event; in this case, correlation maximizes with $\sim 60\%$ connectivity at $t' \sim 25$. The January substorm onset is mainly characterized by fast propagating ($0-6$ minutes lag) connections whilst in the multi-event mean sub-network $\sim 80\%$ of connections are propagating (non-zero peak lag) throughout. This is consistent with a pattern that is both coherent and propagating and/or expanding. The timings of region B growth are consistent across the majority of substorms observed.

About 10 normalized minutes after onset we can see in panel 6 westward propagation and/or expansion from region B (around onset) into region A (westward of onset), B→A. This coincides with an increase in spatial correlation within region A (panel 2). For both the individual and the multi-event average, the B→A time series (panel 6), that is, the relative increase in the number of connections at different lags, resembles that of the network located wholly within region B (panel 3), except that it occurs ~ 10 normalized minutes later and has about half the magnitude. Within region A (panel 2), $\sim 50\%$ of magnetometers become highly correlated at $20 < t' < 30$. For the individual substorm most of the connections between magnetometers are instantaneous, but for the multi-event average $\sim \frac{2}{3}$ of the increase in the number of connections is at non-zero lag. We have found some variation between individual substorms as to how spatial correlation between magnetometers within region A develops from $-10 \leq t' \leq 50$, with some substorms having no obvious response to onset. The A→B (panel 5) propagation and/or expansion develops on similar timescales to B →A (panel 6) but there are significantly fewer connections ($20-30\%$ of magnetometers correlated at peak, $t' = 30$) within the multi-event average, with $\sim \frac{1}{3}$ of these connections being instantaneous (zero lag, no direction).

The sub-network for region C (panel 4, east of the SCW) has the smallest response to substorm onset of any region. The January substorm remains moderately connected ($\sim 23\%$) from before onset until long after peak expansion. The multi-event average begins to increase at $10 < t' < 20$ and the region is maximally correlated after peak expansion, $t' > 30$ with $\sim 20\%$ of magnetometer pairs being connected; this pattern of correlation is consistent long into the recovery phase. This is consistent with many of the individual substorms showing little/no response to onset. In panel 9 we see that region B becomes correlated with region C with eastwards propagation and/or expansion (B→C) $\sim 10-20$ normalized minutes after onset, peaking with $\sim 20\%$ magnetometer pairs correlated at $t' > 30$. In panel 10, we can see that for the individual event $< 10\%$ of magnetometers are correlated from C→B, with this small increase only occurring ~ 25 normalized minutes after onset. Correlation increases by $\sim 15\%$ for the multi-event average between $t' \sim 10$ and $t' \sim 30$. Thus the response within region C simply tracks that of the propagation or expansion from B → C, and any propagation from C → B occurs subsequently.

Finally, $\sim 10 - 20$ normalized minutes after onset, in panels 7 and 8 we see correlation growing relatively slowly between regions A and C (west and east of the onset location, respectively), reaching a maximum level of connectedness at $t' \sim 40$, long af-

ter the time of peak expansion. There is slightly more eastward propagation (A→C, > 20% of magnetometers) than westward propagation (C→A, ∼ 10% and ∼ 18% of magnetometer pairs for the individual and multi-event average, respectively). Again, the lagged correlation originating in C is very small (and mostly instantaneous) for the individual event.

4.2 Interpretation

If we can interpret coherent patterns of spatial correlation across the distributed SuperMAG magnetometers as the emergence of current systems, the above time-dependent network provides an evolution sequence, with timings, for the substorm current system in the nightside. Our analysis then provides a quantitative measure of spatial coherence as well as the time scales on which evolution occurs. By separating the nightside into three regions we have attempted to isolate the components that have been proposed. To use the terminology of Kamide and Kokubun (1996) we have: (A) eastward electrojet; (B) substorm unloading component (SCW) and (C) westward electrojet. Whereas B is associated with the substorm current wedge, or DP1 perturbations, A and C can be related to the general magnetospheric convective system, DP2 (Nishida, 1968), which is enhanced during substorm growth and expansion phases (Milan et al., 2017). To summarize the above results we identify key time ranges, before and after onset: $0 \leq t'_1 < 10$, $10 \leq t'_2 < 20$, $20 \leq t'_3 < 30$ and $t'_4 \geq 30$ in terms of normalized time, t'. Relating these intervals to substorm evolution t'_1 is following onset, t'_2 is expansion phase, t'_3 is near substorm peak and t'_4 is the early recovery phase. The timings are:

- Before onset, the pre- and post-midnight regions A and C each have a relatively weak coherent pattern consistent with convection (DP2); notably A and C are not coherent with each other.
- In t'_1 we first see the formation of a substorm current wedge (SCW/DP1) around onset (correlation within B) which approaches maximum in t'_2.
- In t'_2 there is westward propagation and/or expansion of the SCW west towards the pre-midnight region (A). We see connections (B→A) and at the same time a signature of a coherent current system within region A (correlation within A). This is shortly followed by weaker correlation from A→B, indicating that the entire A-B system is now correlated. These all approach a maximum at t'_3.
- A weaker signal of eastward propagation and/or expansion of the SCW towards the post-midnight region starts in t'_2, and reaches its maximum in t'_4. We see connections (B→C) and on a similar timescale a signature of a coherent current system within region C (correlation within C), with additional weaker correlation from C→B. The correlation in region C is relatively low.
- The regions eastward and westward of onset (A and C) each have a coherent pattern consistent with enhanced magnetospheric convection (DP2). Later in the substorm there is coherence between regions A and C, beginning well after onset, in t'_2, and reaching maximum correlation in t'_4, that is, only after region B has become correlated with all other regions. This can either reflect direct correlation between A and C, or could simply imply that both A and C are correlated with B.

We can then consider what support these results provide for proposed models for substorm current systems, specifically, models with a single westward electrojet segment (Kamide & Kokubun, 1996; McPherron et al., 1973), a westward and, a lower (but still in the auroral zones) latitude eastward electrojet segment (Ritter & Lühr, 2008; Sergeev et al., 2014, 2011); two unconnected westward electrojet segments pre- and post-midnight (Gjerloev & Hoffman, 2014; Rostoker, 1996) and finally many small individual segments (Liu et al., 2018). Importantly, any method for quantifying spatial correlation cannot distinguish between direct correlation (here, A→C) and indirect correlation (here, A→B→C);

this indirect correlation may enhance the number of A→C connections relative to B→C. Therefore our results are not inconsistent with multiple separate current systems provided that they are either spatially correlated with each other, or on spatial scales smaller than that of the magnetometer spacing.

The coherent patterns of eastward and westward expansion are in agreement with previous work using synchronous space and ground based magnetometers (Nagai, 1982, 1991). However, we have not found definitive support for two, or more, distinct and uncorrelated substorm current systems. A lag, $\mid \tau_c \mid > 0$, for B→C connections, implies that C is delayed with respect to B, consistent with a propagation from B to C. Interpreting these results in terms of current components suggest two scenarios for this propagation: i) a single current segment which is expanding from B to C; or, ii) a current segment in B and another in C, where the segment in C is correlated with that in B but is developing with some delay. There is no interpretation of our results which would suggest a scenario where regions B and C are uncorrelated, independent current systems.

If they are associated entirely with general magnetospheric convection (DP2 system), the pre- and post- midnight (A and C) are directly-driven by the solar wind and must enhance on similar time-scales, although the magnitudes may differ (Kamide & Kokubun, 1996). We have found that pre-onset, the regions A and C each have coherent, but relatively small, signatures of correlation with little CCC between them. Post-onset, in both the individual event and the average over 86 substorms, the long range east to west (A→C) correlation patterns only emerge after the growth of the SCW (region B). The growth of spatially coherent patterns appears first in B (the SCW, at onset) followed by A (with correlation between B and A) and later, in C. This suggests that following onset, A and C are not solely attributable to enhanced convection and the presence of contemporaneous B → C and B→ A connections suggests that there may be a combination of contributions from convection enhancement and SCW expansion. Importantly, this does not require that a current segment in A expands or propagates into C.

Finally, if instead of a large scale SCW there were only many small, uncorrelated, individual segments (Liu et al., 2018) we would not expect to find the long-range correlations (A to C) seen here (also SI, figure 1). Since we calculate CCC on minute resolution time series, each connection in the network is derived from a 128 minute time window. Thus we cannot resolve short-timescale events such as a large number of small wedgelets each associated with a bursty bulk flow (BBF) in the plasma sheet which have lifetimes of some 10 min. In addition, we cannot resolve structures that are on smaller spatial scales than the inter-magnetometer spacing. If multiple wedgelets are present, their spatial aggregate would give an overall large-scale magnetic amplitude signature mainly at the edges of the region containing the wedgelets, regardless of whether or not the wedglets are spatio-temporally correlated. Here, both spatial and temporal information is used to obtain the cross-correlation so that temporally uncorrelated wedgelets would give no spatially coherent signature of cross correlation at all, whereas if the same wedgelets were temporally correlated, we would find a signature of spatial cross-correlation.

Potential limitations to the technique include sensitivity to the location of the east and west bulge boundaries, which are static and therefore may not fully represent fast changes in the time-varying current system. There may also be a spatial coarse-graining effect due to the geographic location of the finite number of magnetometers; there are few near the eastward SWC boundary during the January substorm. To test this we present the same plots for this event, but with the east and west boundaries of the bulge at $t' = 15$ and $t' = 45$ in the SI. These show little change from the results shown in Figure 2. Additionally, the detailed network maps of the individual event, for the times represented by the vertical dashed lines in Figure 2, onset-peak, are provided in the SI. They highlight the importance of the spatial coverage and geographical locations of the highly correlated magnetometer pairs.

Also, in the analysis and by the organization of data into three regions, A, B, C, we are quantifying the coherence over these regions. This is over a range in both latitude ($60 - 75^\circ$) and local time (typically region B is ~ 6 hrs LT). The westward electrojet around onset (B) may not cover all latitudes but our analysis technique is mainly addressing the various SCW models which differ in their local time distribution.

5 Conclusions

We used the full set of SuperMAG ground-based magnetometer observations of isolated substorms to quantify the time evolution of patterns of spatial correlation. If the observed pattern of spatial correlation between magnetometer observations captures ionospheric current patterns then we can directly test different models for substorm ionospheric current systems. We have obtained the first directed networks for isolated substorms. Each connection in the network indicates when the maximum canonical cross-correlation CCC between the vector magnetic field perturbations seen at each pair of magnetometers exceeds an event and station specific threshold. The maximum of the CCC corresponding to each connection in the network can occur at a non-zero time lag. The resulting *directed* network then contains information, not only on the formation of coherent patterns seen by multiple magnetometers, but also on the propagation and/or expansion of these spatially coherent structures.

To gain insight on the ionospheric current system during a substorm, we obtained specific time-varying sub-networks from the data which isolate specific physical regions. These regions are west (A), within (B) and east (C) of the bulge boundaries for each substorm (obtained from polar VIS images at the time of peak expansion). We presented both a study of an individual event, which has at least seven magnetometers in each of these regions for the duration of the substorm, as well as the average of the network properties of 86 substorm events. If the observed pattern of spatial correlation between magnetometer observations captures ionospheric current patterns, we find the following sequence of events in terms of key time ranges after onset: $0 \leq t'_1 < 10$, $10 \leq t'_2 < 20$, $20 \leq t'_3 < 30$ and $t'_4 \geq 30$ (t' is normalized time (Gjerloev et al., 2007)):

- Pre- onset, the pre- and post-midnight regions A and C each have a relatively weak coherent pattern consistent with general magnetospheric convection (DP2) and are not coherent with each other.
- A dominant substorm current wedge (SCW) forming around the onset location (within region B) at the time of onset, t_1, which reaches maximum spatial correlation at t_2, half way through the expansion phase.
- This is followed by a westward expansion of this SCW (starting at t_2, with peak at t_3) contemporaneous to and coherent with a current system in the pre-midnight region (within A).
- An additional weaker eastward expansion of the SCW (starting slowly at t_2 with peak at t_4). The signal of a self-contained current post-midnight (region C) is relatively weaker and occurs late in the substorm. The enhancement of C is delayed with respect to that of A.
- Following the SCW expansion, A and C are coherent with each other, but at the same time are coherent with the SCW. This is consistent with a combination of convection and expansion of the SCW.

These conclusions are drawn from the averaged network over 86 isolated substorms. Although the overall spatio-temporal timings revealed by this network analysis are reasonably consistent between individual events and the 86 event average for the formation of a SCW around onset (B) and it's expansion both east (B→C) and west (B→A), the exact timings of the current system evolution varies. Variability between events could be intrinsic or could relate to the observing conditions, such as differing magnetometer

spatial coverage or the static choice of location for region boundaries. Future work will quantify event-by-event variability across multiple events and extend the analysis to multiple, compound events. So far in our analysis we have not utilized the direction of the (vector) maximal CCC. In principle this could resolve the direction of the electojet (eastward/westward).

Acknowledgments

We acknowledge use of the SuperMAG ground magnetometer station data from `http://supermag.jhuapl.edu/` and thank Rob Barnes for providing us with a hard copy (Dec 2017). S. C. C acknowledges a Fulbright-Lloyds of London Scholarship, AFOSR grant FA9550-17-1-0054 and STFC ST/P000320/1. We thank the Santa Fe Institute for hosting a visit during which we worked on this research.

References

Akasofu, S.-I. (1964). The development of the auroral substorm. *Planetary and Space Science*, *12*(4), 273–282.

Albert, R., & Barabási, A.-L. (2002). Statistical mechanics of complex networks. *Reviews of modern physics*, *74*(1), 47.

Boccaletti, S., Latora, V., Moreno, Y., Chavez, M., & Hwang, D.-U. (2006). Complex networks: Structure and dynamics. *Physics reports*, *424*(4-5), 175–308.

Dods, J., Chapman, S., & Gjerloev, J. (2015). Network analysis of geomagnetic substorms using the supermag database of ground-based magnetometer stations. *Journal of Geophysical Research: Space Physics*, *120*(9), 7774–7784.

Dods, J., Chapman, S., & Gjerloev, J. (2017). Characterizing the ionospheric current pattern response to southward and northward imf turnings with dynamical supermag correlation networks. *Journal of Geophysical Research: Space Physics*, *122*(2), 1883–1902.

Gjerloev, J. (2012). The supermag data processing technique. *Journal of Geophysical Research: Space Physics*, *117*(A9).

Gjerloev, J., & Hoffman, R. (2014). The large-scale current system during auroral substorms. *Journal of Geophysical Research: Space Physics*, *119*(6), 4591–4606.

Gjerloev, J., Hoffman, R., Sigwarth, J., & Frank, L. (2007). Statistical description of the bulge-type auroral substorm in the far ultraviolet. *Journal of Geophysical Research: Space Physics*, *112*(A7).

Jost, J. (2007). Dynamical networks. In *Networks: from biology to theory* (pp. 35–62). Springer.

Kamide, Y., & Kokubun, S. (1996). Two-component auroral electrojet: Importance for substorm studies. *Journal of Geophysical Research: Space Physics*, *101*(A6), 13027–13046.

Kullen, A., & Karlsson, T. (2004). On the relation between solar wind, pseudobreakups, and substorms. *Journal of Geophysical Research: Space Physics*, *109*(A12).

Liu, J., Angelopoulos, V., Yao, Z., Chu, X., Zhou, X.-Z., & Runov, A. (2018). The current system of dipolarizing flux bundles and their role as wedgelets in the substorm current wedge. *Electric Currents in Geospace and Beyond*, 323–337.

Malik, N., Bookhagen, B., Marwan, N., & Kurths, J. (2012). Analysis of spatial and temporal extreme monsoonal rainfall over south asia using complex networks. *Climate dynamics*, *39*(3-4), 971–987.

McGranaghan, R. M., Mannucci, A. J., Verkhoglyadova, O., & Malik, N. (2017). Finding multiscale connectivity in our geospace observational system: Network analysis of total electron content. *Journal of Geophysical Research: Space Physics*, *122*(7), 7683–7697.

McPherron, R. L., Russell, C. T., & Aubry, M. P. (1973). Satellite studies of magnetospheric substorms on august 15, 1968: 9. phenomenological model for substorms. *Journal of Geophysical Research*, *78*(16), 3131–3149.

Milan, S. E., Clausen, L. B. N., Coxon, J. C., Carter, J. A., Walach, M.-T., Laundal, K., ... others (2017). Overview of solar wind–magnetosphere–ionosphere–atmosphere coupling and the generation of magnetospheric currents. *Space Science Reviews*, *206*(1-4), 547–573.

Nagai, T. (1982). Observed magnetic substorm signatures at synchronous altitude. *Journal of Geophysical Research: Space Physics*, *87*(A6), 4405–4417.

Nagai, T. (1991). An empirical model of substorm-related magnetic field variations at synchronous orbit. *Washington DC American Geophysical Union Geophysical Monograph Series*, *64*, 91–95.

Newman, M. E. (2003). The structure and function of complex networks. *SIAM review*, *45*(2), 167–256.

Nishida, A. (1968). Coherence of geomagnetic dp 2 fluctuations with interplanetary magnetic variations. *Journal of Geophysical Research*, *73*(17), 5549–5559.

Pulkkinen, A. (2015). Geomagnetically induced currents modeling and forecasting. *Space Weather*, *13*(11), 734–736.

Reinsel, G. C. (2003). Review of canonical correlations in multivariate analysis. In *Elements of multivariate time series* (p. 68-70). Springer Science & Business Media.

Richmond, A., & Kamide, Y. (1988). Mapping electrodynamic features of the high-latitude ionosphere from localized observations: Technique. *Journal of Geophysical Research: Space Physics*, *93*(A6), 5741–5759.

Ritter, P., & Lühr, H. (2008). Near-earth magnetic signature of magnetospheric substorms and an improved substorm current model. In *Annales geophysicae* (Vol. 26, pp. 2781–2793).

Rostoker, G. (1996). Phenomenology and physics of magnetospheric substorms. *Journal of Geophysical Research: Space Physics*, *101*(A6), 12955–12973.

Sergeev, V., Nikolaev, A., Tsyganenko, N., Angelopoulos, V., Runov, A., Singer, H., & Yang, J. (2014). Testing a two-loop pattern of the substorm current wedge (scw2l). *Journal of Geophysical Research: Space Physics*, *119*(2), 947–963.

Sergeev, V., Tsyganenko, N., Smirnov, M., Nikolaev, A., Singer, H., & Baumjohann, W. (2011). Magnetic effects of the substorm current wedge in a spread-out wire model and their comparison with ground, geosynchronous, and tail lobe data. *Journal of Geophysical Research: Space Physics*, *116*(A7).

Stolbova, V., Tupikina, L., Bookhagen, B., Marwan, N., & Kurths, J. (2014). Topology and seasonal evolution of the network of extreme precipitation over the indian subcontinent and sri lanka. *Nonlinear Processes in Geophysics*.

Tanskanen, E., Pulkkinen, T., Koskinen, H., & Slavin, J. (2002). Substorm energy budget during low and high solar activity: 1997 and 1999 compared. *Journal of Geophysical Research: Space Physics*, *107*(A6).

Watts, D. J., & Strogatz, S. H. (1998). Collective dynamics of small-worldnetworks. *nature*, *393*(6684), 440.

Wiedermann, M., Radebach, A., Donges, J. F., Kurths, J., & Donner, R. V. (2016). A climate network-based index to discriminate different types of el niño and la niña. *Geophysical Research Letters*, *43*(13), 7176–7185.

Figure 1.

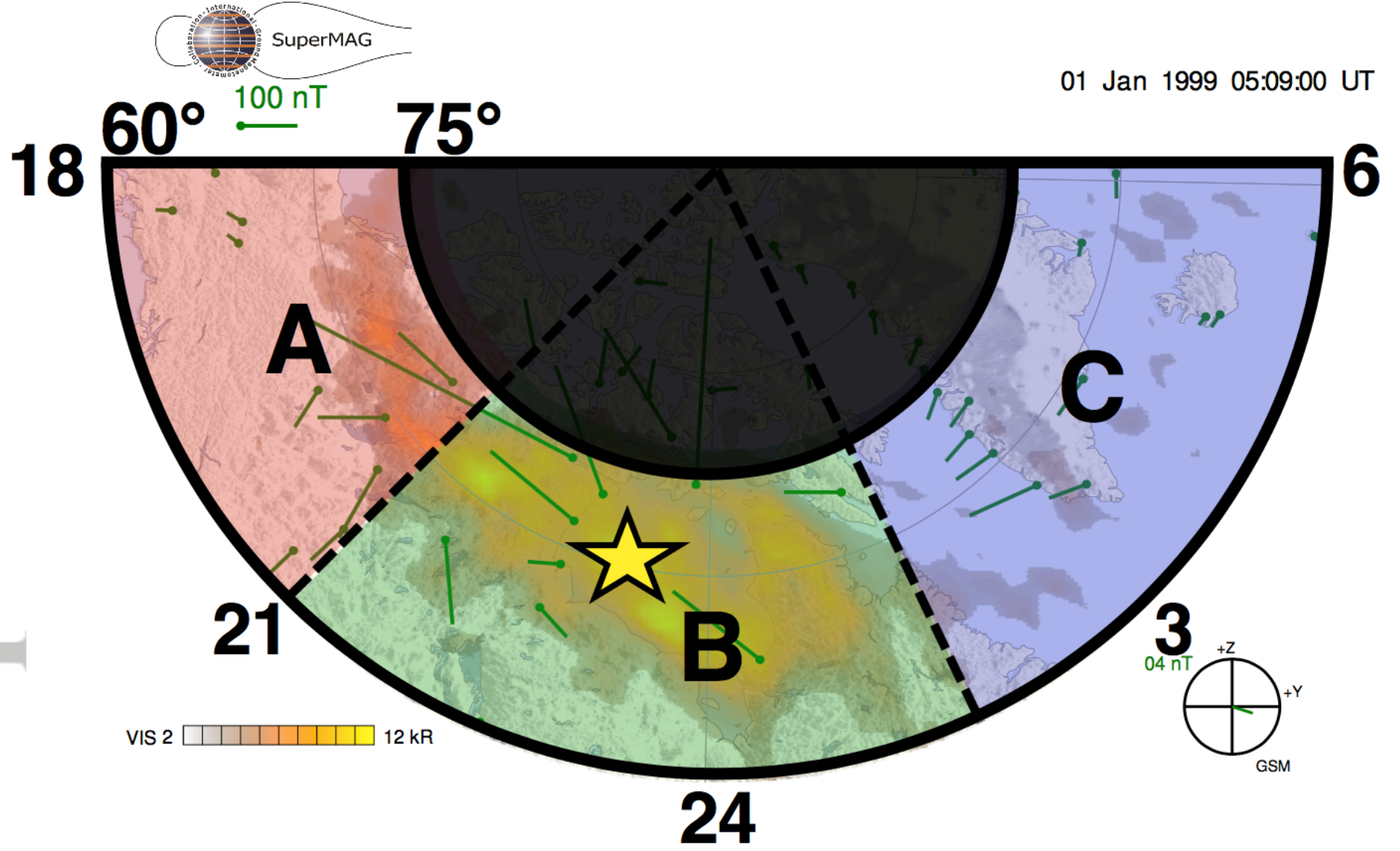
SuperMAG
100 nT
01 Jan 1999 05:09:00 UT
60°
75°
18
6
A
B
C
21
3
24
04 nT
+Z
+Y
GSM
VIS 2
12 kR

Figure 2.

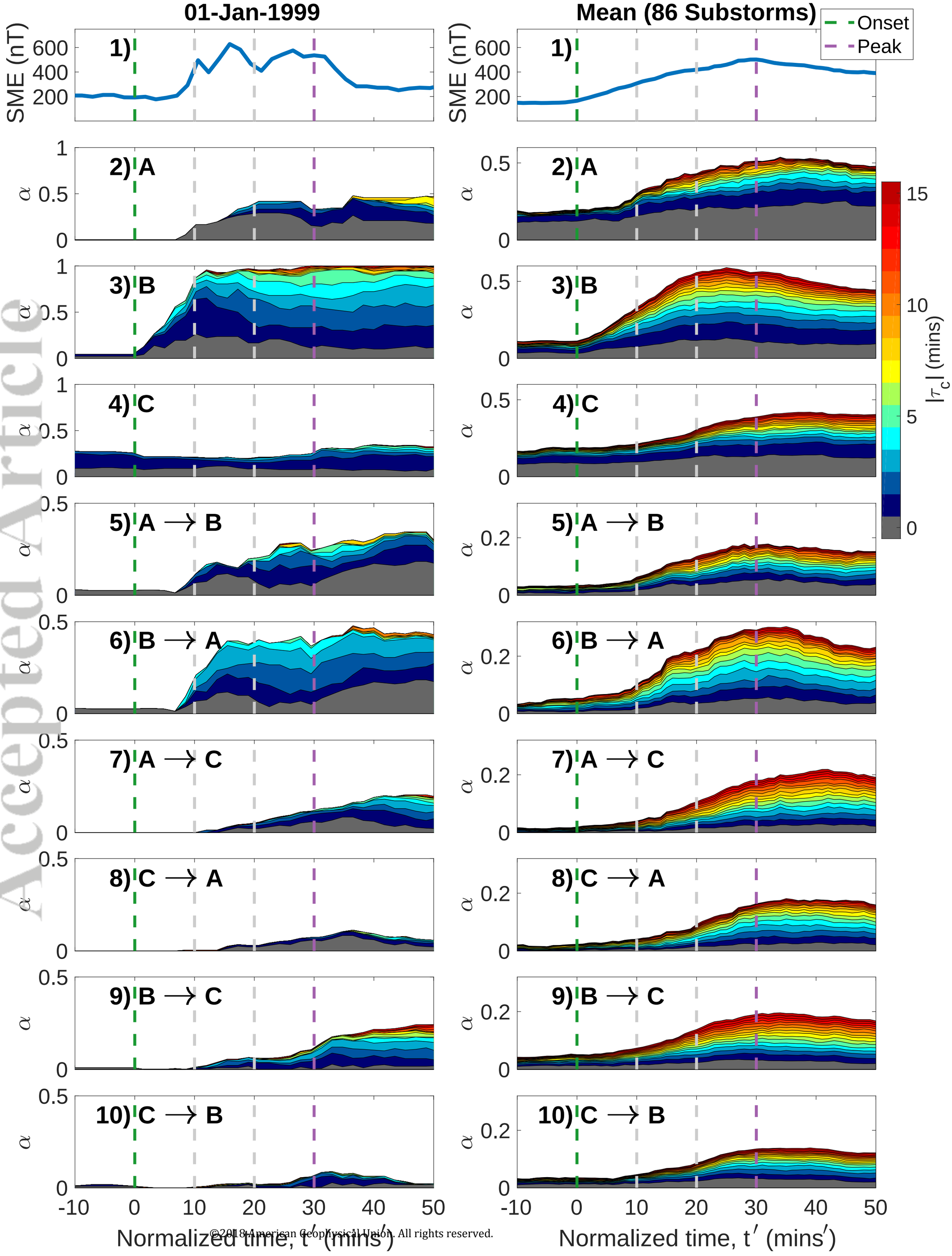

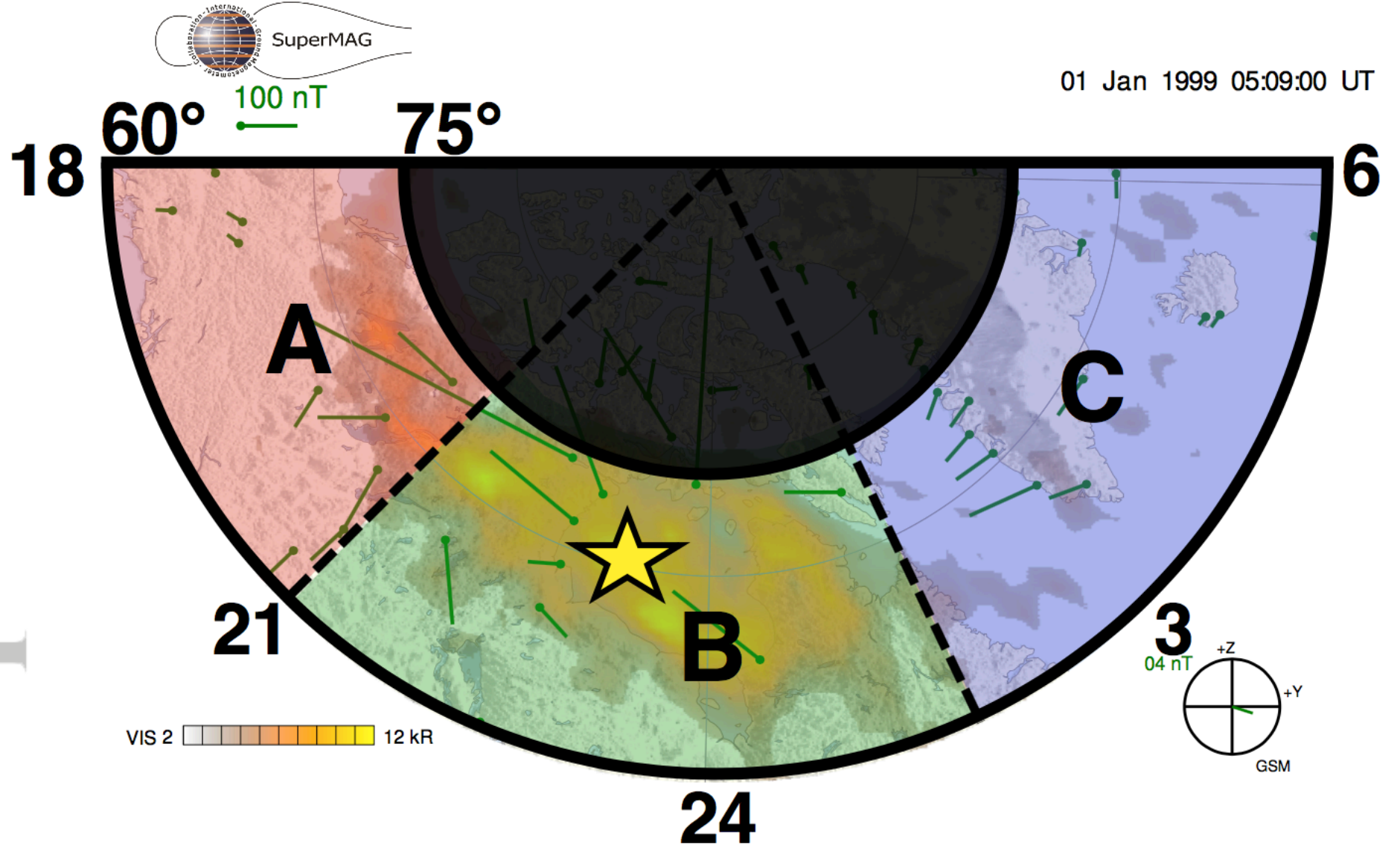
SuperMAG
100 nT
01 Jan 1999 05:09:00 UT
60°
75°
18
6
A
B
C
21
3
24
04 nT
+Z
+Y
GSM
VIS 2
12 kR